iScience

Article

Soft wearable thermo+touch haptic interface for virtual reality

Graphical abstract

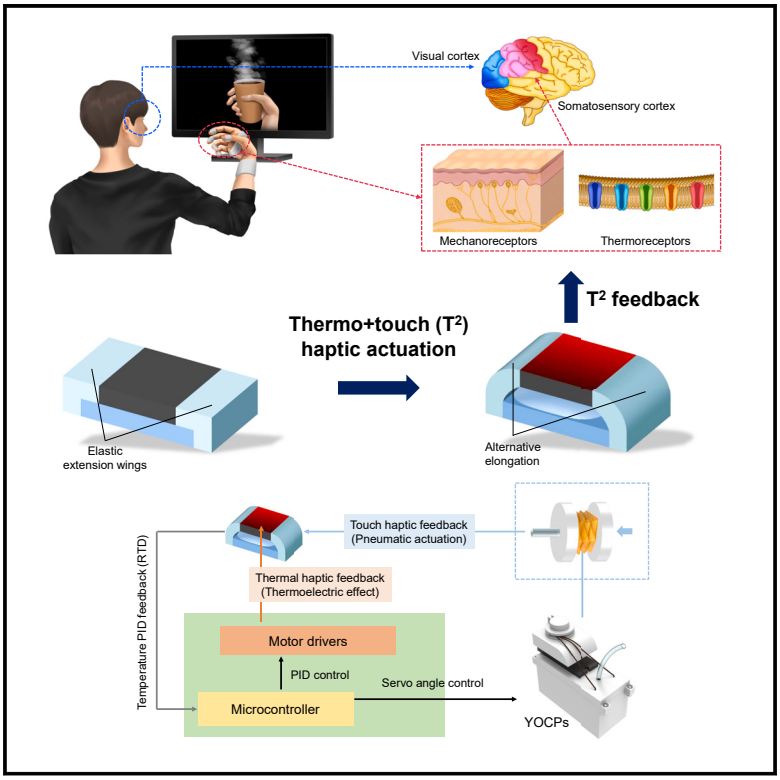

Highlights

- Soft, wearable, and multimodal thermotouch haptic feedback device
- Haptic actuator with a specially designed soft pneumatic-thermoelectric module
- Integral haptic interface with the haptic feedback device and a real-time VR environment

Authors

Seohu Lee, Seongkwan Jang, Youngsu Cha

Correspondence

ys02@korea.ac.kr

In brief

Natural sciences; Applied sciences; Robotics

Lee et al., 2024, iScience *27*, 111303
December 20, 2024
https://doi.org/10.1016/j.isci.2024.111303

CellPress

iScience

CellPress
OPEN ACCESS

Article

Soft wearable thermo+touch haptic interface for virtual reality

Seohu Lee,[1] Seongkwan Jang,[2] and Youngsu Cha[1,3,*]
[1]School of Electrical Engineering, Korea University, 145 Anam-ro, Seongbuk-gu, Seoul 02841, South Korea
[2]School of Mechanical Engineering, Korea University, 145 Anam-ro, Seongbuk-gu, Seoul 02841, South Korea
[3]Lead Contact.
*Correspondence: ys02@korea.ac.kr
https://doi.org/10.1016/j.isci.2024.111303

SUMMARY

Touch is an inherent source of tactile sensation in everyday life, followed by vision and audition. For rich tactile feedback, multimodal haptic feedback is necessary because a single touch simultaneously excites multiple types of tactile receptors. In this paper, we present a soft wearable thermotouch haptic interface (T^2HI) that simultaneously and independently provides touch and thermal stimulation using only one end-effector, the thermotouch haptic actuator (T^2HA). A T^2HA consists of a pneumatic-based touch haptic actuator and a thermoelectric-based thermal haptic stimulator. A novel design for the harmonious integration of the two different parts with wearable air pumps was proposed. Finally, the efficacy of the T^2HI with virtual reality (VR) was evaluated by a user test. In VR, users manipulated a virtual object, and the corresponding touch and thermal feedback were provided. The T^2HI demonstrated that multimodal haptic feedback significantly enhances the VR engagement of users compared to single-modal feedback.

INTRODUCTION

Perception is the process of sensory interpretation to understand the present.[1] Touch is the source of tactile sensation that facilitates perception of the surface properties (e.g., temperature and texture) and motion states (e.g., vibration) of objects,[2,3] in addition to vision and audition. This physiological feature has provoked vigorous studies in the field of haptics,[4–8] which is a common term embracing both tactile and kinesthetic modalities.[9]

The tactile modality is addressed in this study. Tactile sensory information is primarily received by two types of cutaneous receptors in the dermis: mechanoreceptors and thermoreceptors.[9] Among various mechanisms of haptic actuators,[6,7,10] pneumatic actuation and thermoelectric effect were chosen as the base mechanism. Vibrotactile actuation could have been a strong candidate thanks to its instantaneous response and simpler system, but the lack in force and displacement (approximately 1/10 times compared to normal indentation[11]) had been unfavorable. The advantages of pneumatic actuators, including high power output, lightweight design, cleanliness, and safety,[12,13] as well as the benefits of thermoelectric devices (TEDs), such as their high coefficient of performance and the ability to be fabricated in thin and flexible structures,[14] make them favorable for soft wearable devices.

Pneumatic actuators have demonstrated their versatility as soft wearable haptic devices with many applications.[15–23] The most common type of application is simple indentation on the skin.[16–22] Vibrotactile feedback using pneumatic vibrators has also been studied.[15–17,19,20] Beyond the simple vibrotactile, an advanced shear-sliding haptic renderer was also presented.[23] TEDs also have demonstrated their feasibility as soft wearable thermal displays.[24–30] The bi-functional (heating/cooling) utility with simple current reversing is one of the competitive features of TEDs.[24–28] Additionally, conformal contact, thanks to the softness, remarkably enhances thermal sensation by reducing the thermal resistance between the device and the skin.[28]

Furthermore, with the recent progress in computer technologies, the distinction of haptic perception over visual and auditory perception has highlighted their synergistic effects with virtual reality (VR) and augmented reality (AR).[6,7,11,14–18,24,25,30–34] Particularly, VR/AR with soft or on-skin devices is favored for wearables, compared to conventional rigid ones.[33,34] Many VR/AR with soft haptic interface have been reported in the aspects of thermal,[14,24,25,30] indentation,[16–18] vibrotactile,[15–18,31] and integrated thermovibrotactile[32] haptics.

Despite these active studies, few reports that combine pneumatic actuators and TEDs for simultaneous force and thermal haptic stimulations could be found, although each of them has been preferably used. Instead, some studies using indirect methods could be found. Cai et al.[35] and Lee et al.[36] heated or cooled air in a chamber and supplied the air to the device. This mechanism indirectly relays thermal feedback along with pneumatic actuation. Furthermore, most commercial VR/AR experiences (e.g., movies and games) are still limited to visual and auditory feedback, with only a few simple applications with vibration feedback.[37] The absence of full system-level haptic implementation is presumably because of insufficient haptic feedback, low portability (e.g., air compressors), and component-level focused

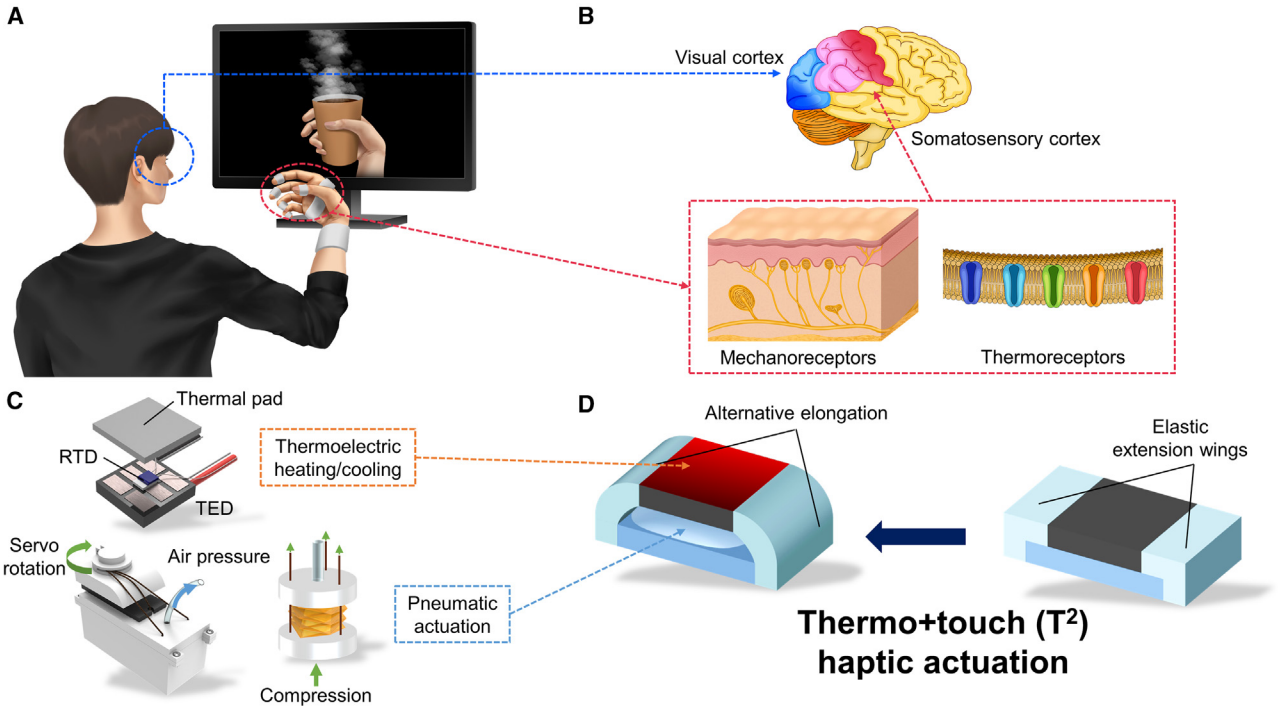

Figure 1. Schematic of the T²HI

(A) VR interaction. A human grabs a virtual hot coffee cup.

(B) Perception mechanism. Visual and mechanical/thermal tactile sensation reaches the visual and somatosensory cortex, respectively.

(C) Operation mechanism of the T²HA.

(D) Actuation of the T²HA.

development.[11,37,38] Current progress in haptic interfaces suggests the necessity for high-quality haptic feedback, high portability, and full-system-scale haptic interface development for future commercialization.[35,39]

In this paper, we propose a novel-design soft wearable thermotouch haptic interface (T²HI) that can provide both touch and thermal stimulation independently and simultaneously, in addition to the visual feedback of VR (Figure 1). In VR, users can pinch or grab an object through visual perception, the respondent thermotouch feedback is provided to the fingers, and this feedback is sensed by cutaneous receptors and perceived by the somatosensory cortex (Figures 1A and 1B). The interaction is encoded into serial data in VR, and the contact data are wirelessly transmitted to a microcontroller attached to the user via Bluetooth communication. The data are decoded in the microcontroller, and the decoded data are translated into the operational statement of the thermotouch haptic actuator (T²HA).

The T²HA consists of two parts: a pneumatic-based touch haptic actuator and a thermoelectric-based thermal haptic stimulator (Figure 1C). Functional and structural synergy for effective feedback and good wearing comfort should be profoundly considered for multimodal integration.[6] We solved this problem by a novel design: the elastic extension of a thermal haptic stimulator. The T²HA was designed as a two-layer structure with a touch haptic actuator under an elastically extended thermal haptic stimulator (Figure 1D). Two wings made of highly elastic silicone rubber were attached to both sides of the TED of the thermal haptic stimulator to allow free TED movement. The additional elastic margin helps mediate the pneumatic inflation of the below touch haptic actuator across the thermal haptic stimulator with alternating elongation of the wings. This design overcomes the inelasticity of the TED while maintaining the pneumatic actuation. In turn, the thermal haptic stimulator becomes the bimodal end-effector of the T²HA.

Additionally, a wearable air pump and a pneumatic actuator were specially designed to reduce the bulkiness. The pump was designed inspired by the previous study in our research group, which developed a tendon-driven origami pump to replace bulky air regulators.[40] The Yoshimura origami pattern was chosen for a Yoshimura origami cylindrical pump (YOCP), inspired by the natural buckling of cylindrical shells under axial loading.[41] The pump can be self-released thanks to its inherent elastic deformation for being folded.[42] Consequently, the pump can be controlled by the tension of a tendon; the elimination of releasing mechanism simplifies the system. However, isolation from the atmosphere limits its air supply capacity. We solved this challenge by a special design: a zero-dead-volume pneumatic actuator. Pneumatic actuators operate with volumetric change of gas.[6] Thus, the zero dead volume maximizes the volumetric ratio change; in turn, the pressure is maximized. Furthermore, the zero dead volume minimizes the thickness of the T²HA, which enhances wearability and comfort.

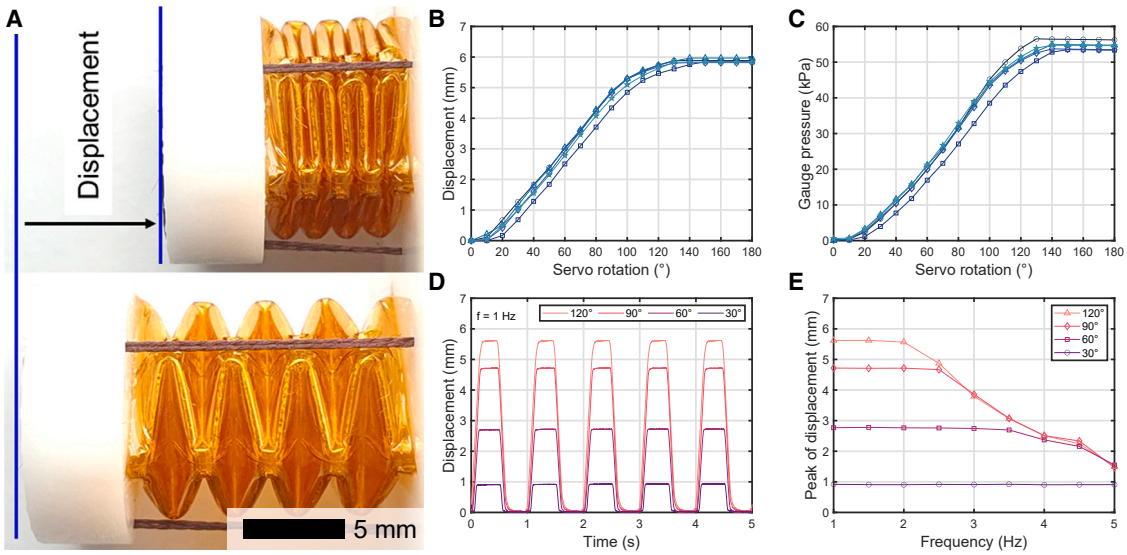

Figure 2. Evaluation of the YOCP

(A) Compression motion of the YOCP.

(B) Displacement of the YOCP with the servo rotation.

(C) Gauge pressure of the YOCP with the servo rotation.

(D) Dynamic operation of the YOCP at 1 Hz repetition. The servo rotation amplitudes are 30°, 60°, 90°, and 120°.

(E) Frequency response of the YOCP from 1 to 5 Hz for the same rotation ranges.

RESULTS

In this section, we evaluate the performances of YOCP and T^2HA. We conducted a user test to demonstrate the efficacy of the multimodal haptic feedback of the T^2HI compared with a single touch or thermal haptic feedback. Experiments, results, and discussion are presented in this section.

YOCP evaluation

Manipulation

The YOCP pressure is determined by the displacement of the pump (Figure 2A). The displacement is controlled by the length of a tendon, and the length of the tendon is controlled by a servo. Therefore, the key manipulating factor for YOCP is the servo rotation.

The displacement of the YOCP was measured using a laser sensor (IL-100 CMOS multifunction analog laser sensor, Keyence Co., Japan). The initial length of the YOCP is 20 mm, which is determined by the housing of the YOCP. The laser beam reached the YOCP plug through a hole at the bottom of the housing. The results for five samples are shown in Figure 2B. The displacement of the YOCP was analyzed by dividing it into four ranges approximately 0°–20°, 20°–100°, 100°–140°, and 140°–180°. The first region (0°–20°) was the tendon fastening stage. During fabrication, the tendon was not fully tightened and had some initial looseness. The tendon tightened during this stage. The second stage (20°–100°) was the linear compression stage. The length of the tendon was linearly shortened along by servo rotation. The third stage (100°–140°) was the elastic deformation stage. Because the Yoshimura origami cylinder cannot be a rigid-folded structure, elastic deformation is necessary for the transformation of the cylinder.[42] This state occurs when the restoring force against the elastic deformation becomes critical. The final stage (140°–180°) was the maximum compression stage. The restoring force against elastic deformation was equilibrated with the torque of the servo.

Pressure of the YOCP was measured using a pressure sensor (33A-015D-2210, Shiba Korea Co., Ltd., Korea). The voltage output of the sensor was measured using a data acquisition board (DAQ) (DAQ NI-9229, National Instrument Co., USA). The results for the five samples are shown in Figure 2C. The relationship between the pressure and servo rotation was almost the same as that between the pressure and displacement (Figure 2B). The only difference was the nonlinearity in the range of 20°–100°. The results also show that the pressure of the YOCP can be successfully regulated by the servo rotation angle.

Frequency response

The frequency response of YOCP is an important characteristic for pneumatic suppliers. The response describes how effectively and quickly the YOCP accomplishes the desired performance across a range of frequencies.

The dynamic repetition of the displacement was measured using the laser sensor and DAQ. The servo rotation amplitudes were set to 30°, 60°, 90°, and 120° in the experiment. The value of 120° was roughly selected from the previous experiments (Figures 2B and 2C) with some margin for the maximum compression. The repetitive motion of the YOCP at frequency of 1 Hz is shown in Figure 2D. At 1 Hz, YOCP showed stable repetition for all rotation amplitudes. Subsequently, the frequency response of YOCP was tested from 1 to 5 Hz with a 0.5 Hz increment at each step. The results are presented in Figure 2E. From this, the minimum response time of the YOCP was found. The displacement of the YOCP was successfully

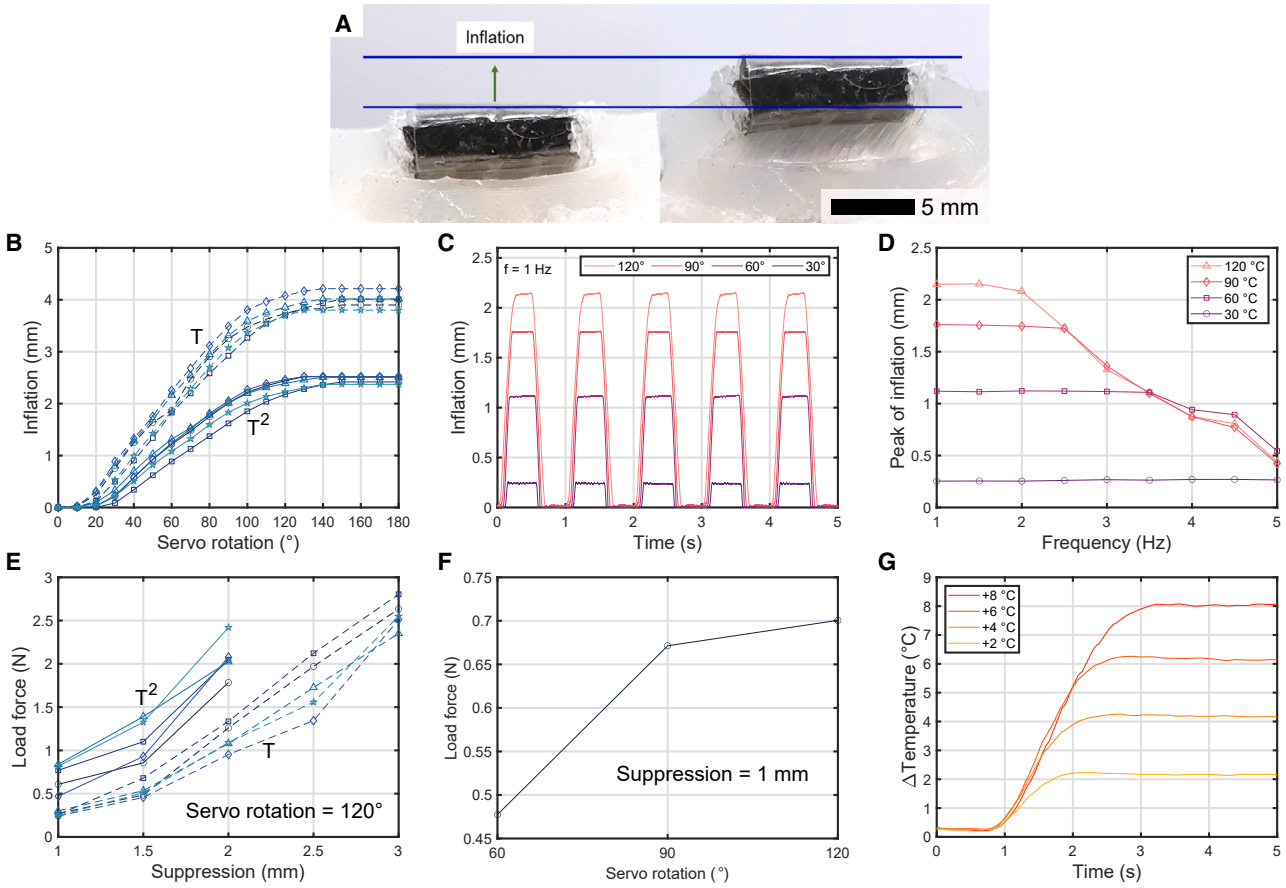

Figure 3. Evaluation of the T²HA

(A) Inflation motion of the T²HA.

(B) Inflation of the T²HA and the touch (T) haptic actuator along with the servo rotation.

(C) Dynamic operation of the T²HA at 1 Hz repetition. The servo rotation amplitudes are 30°, 60°, 90°, and 120°.

(D) Frequency response of the T²HA from 1 to 5 Hz for the same rotation amplitudes.

(E) Load force of the T²HA and the touch (T) haptic actuator against suppression at 120° servo rotation.

(F) Load force of the T²HA along with the servo rotation against 1 mm suppression.

(G) Temperature controllability of the T²HA. The initial temperature was set to 32°C.

saturated up to 2, 2.5, and 3.5 Hz for the 120°, 90°, and 60° rotations, respectively, whereas the 30° rotation maintained saturation in the full range. Therefore, the YOCP required approximately 0.5, 0.4, and 0.3 s (the reciprocal of the frequency) for 120°, 90°, and 60° rotations, respectively.

T²HA evaluation

Manipulation

Touch feedback from the T²HA is generated by pneumatic actuation using the air pressure provided by the YOCP (Figure 3A). In this context, servo rotation is also a key manipulatory factor in the touch feedback of the T²HA.

The pneumatic inflation of the T²HA was measured using a laser sensor. The results for five samples are shown in Figure 3B. The T-denoted dotted lines present the results of the touch haptic actuators. The inflation of the T²HA was reduced compared with that of the touch haptic actuator. Specifically, inflation was reduced by 39% at 120° servo rotation. The relationship between inflation and servo rotation showed the same trend for the YOCP manipulation (Figures 2B and 2C).

Frequency response

The frequency response to T²HA inflation was investigated. Because the T²HA is actuated by a YOCP, the experiments were conducted in the same frequency range as in the previous tests (Figures 2D and 2E).

The dynamic repetition of the inflation was measured using the laser sensor and DAQ. The servo rotation amplitudes were set to 30°, 60°, 90°, and 120°. The repetitive motion of the T²HA at a frequency of 1 Hz is shown in Figure 3C. At 1 Hz, the T²HA still showed stable repetition for all rotation amplitudes. Subsequently, the frequency response of T²HA from 1 to 5 Hz with a 0.5 Hz step showed the same frequency characteristics as YOCP (Figure 3D). Furthermore, the minimum response time for touch haptic actuation of the T²HA was found to be the same as that of the YOCP: approximately 0.5, 0.4, and 0.3 s for 120°, 90°, and 60° rotations, respectively. The result shows

that small rotation angles are preferred for fast response. This can be achieved by increasing the radius of the servo pulley. In that case, reduction in the rotation amplitude may diminish the resolution of touch haptic feedback.

Load force

The ability to provide powerful touch haptic feedback is critical for the optimal performance of the T^2HA. To evaluate these properties, load force generated by the T^2HA was measured.

The load force against suppression was measured using a tensile compression testing machine (MCT-2150, A&D Co., Ltd., Japan). The results for the five samples are shown in Figure 3E; the T-denoted dotted lines present the results of the touch haptic actuators. The reference servo rotation in the experiment was 120°. The suppression was set to 1–3 mm for the touch haptic actuator and 1–2 mm for the T^2HA, with a 0.5 mm step, considering the inflation measured in Figure 3B. The touch haptic actuators produced 0.26, 0.53, 1.14, 1.74, and 2.60 N load forces against suppressions of 1, 1.5, 2, 2.5, and 3 mm, respectively. The T^2HA generated 0.70, 1.12, and 2.07 N load forces against suppressions of 1, 1.5, and 2 mm, respectively. Hence, the load force generated by the T^2HA was approximately 2.66, 2.10, and 1.81 times that generated by the touch haptic actuators against the same suppressions, even though the inflation was reduced. This is because a smaller inflation of the T^2HA was induced by air compression owing to the additional stiffness of the elastic extension wings. Subsequently, the load forces for 60°, 90°, and 120° servo rotations against the same 1 mm suppression were measured (Figure 3F). The load force at 120° was 1.47 times higher than that at 60°.

Temperature regulation

Not only the production but also the control of thermal stimuli is important for a haptic experience. The temperature of T^2HA is controlled by proportional-integral-derivative (PID) control using an interface board that was developed by Lee et al.[26]

The T^2HA includes a resistance temperature detector (RTD) to measure the temperature for feedback from the PID control. The 5.5 V power was supplied by a DC power supply (MK3003P, MKPOWER Co. Ltd., Korea). To verify the temperature controllability at various target levels, a regulation experiment was conducted (Figure 3G). The initial temperature was set to 32°C, and the target temperature was nominally set to 34 (+2)°C, 36 (+4)°C, 38 (+6)°C, and 40 (+8)°C. The 2°C discretion and the maximum 40°C were referenced by the perceptible threshold (1.8°C) and the comfortable heating range (39°C), respectively.[43] The measurement data were smoothed to remove noise using the "smoothdata" function in MATLAB software (MATLAB R2023b, MathWorks Inc., USA). The heating ability of T^2HA was evaluated using three parameters: heating rate, overshoot, and steady-state error. The heating rate is defined as the temperature rise per second within 10%–90% of the increasing range. It was found to be 2.19°C, 3.47°C, 4.55°C, and 4.49°C/s for heating by +2°C, +4°C, +6°C, and +8°C, respectively. Incidentally, the sync of thermotouch is determined by the thermal stimulation rather than the touch, because the respective heating times obtained here are 0.49, 0.69, 0.87, and 1.26 s, which are slower than the minimum pneumatic response times obtained earlier. The overshoot is defined as the maximum excess of the target temperature. It was measured to be 0.23°C, 0.25°C, 0.26°C, and 0.13°C for each target temperature. The steady-state error is defined as the average difference between the actual and target temperatures in a stable region. It was 0.17°C, 0.18°C, 0.15°C, and 0.03°C for the same target temperatures. The cooling ability was evaluated using the same parameters (Figure S1). The initial temperature was set to 32°C, and the target temperature was nominally set to 30 (−2)°C, 28 (−4)°C, 26 (−6)°C, and 24 (−8)°C. However, the temperature could not be regulated properly. The temperature initially dropped down for some time, but a thermal runaway soon occurred.

User test

A user test was conducted to evaluate the efficacy of T^2HI. The test was permitted by the Korea University Institutional Review Board (approval number: KUIRB-2023-0387-01). Twenty participants (10 male and 10 female) participated in the test. The age of the participants was restricted to the 20s based on the progressive reduction in tactile perception with age.[44,45] A 1:1 gender ratio was considered for comparison between sexes based on studies reporting that females are more sensitive to tactile stimuli than males.[45,46] Three T^2HAs were combined and worn by the participants. The end-effectors of the T^2HAs were worn on the thumb, index, and middle fingers. The YOCPs were worn on the back of the backhand. Finally, the interface board was worn on the dorsal forearm. All components were equipped with Velcro bands, considering the different body sizes of participants.

The operation of the T^2HI is shown in Figure 4. Infrared images showing simultaneous thermotouch haptic actuation were captured using an infrared camera (FLIR A-700, FLIR Systems Inc., USA); see Figures 4A–4C. In VR, a dynamically interacting object was created for VR interaction (Figure 4D). The hand motion of a user test was tracked by a portable hand tracking device (Leap Motion Controller, LeapMotion, Inc., USA), and the virtual hand physically interacted with the object in the VR; for example, it could pinch or grab an object (Figures 4E–4G). The corresponding touch and thermal feedback were then provided by the T^2HAs (Figures 4H–4J).

Prior experience

The participants completed a survey regarding their prior haptic (Figure 5A) and VR (Figure 5B) experiences. Four out of the 20 participants (2/10 males and 2/10 females) had experienced a haptic device, and all the four answered that they had experienced vibration haptic feedback (Figure 5A). All the four had experienced touch or thermal haptic feedback, and none had experienced thermotouch. Fourteen of the 20 participants (6/10 males and 8/10 females) had experienced VR. However, no participants had experienced VR that uses haptic feedback.

Evaluation

To validate the efficacy of the T^2HI, a user test was conducted in three stages: only-touch, only-thermal, and thermotouch. In VR, balls with three different colors corresponding to the temperature were provided for VR interaction, based on a previous study showing that color stimuli enhance the recognition of thermal feedback.[24] In the only-touch stage, a gray-colored ball was provided for the VR interaction. Touch feedback was provided at two levels: light and deep touch. In the only-thermal stage, an orange- and a red-colored ball were provided as warm (37°C) and hot (40°C) objects, respectively. Only warm and hot thermal

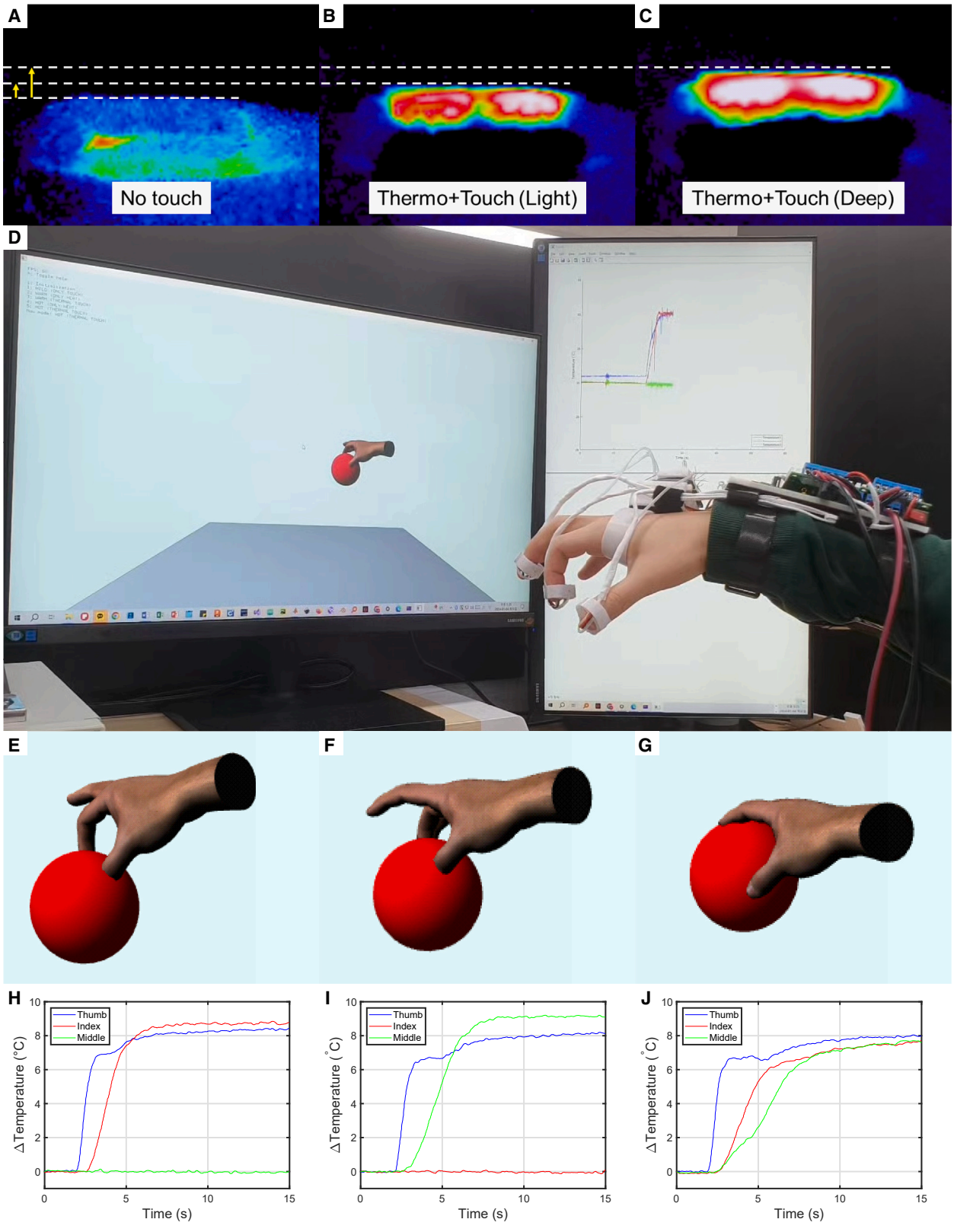

(legend on next page)

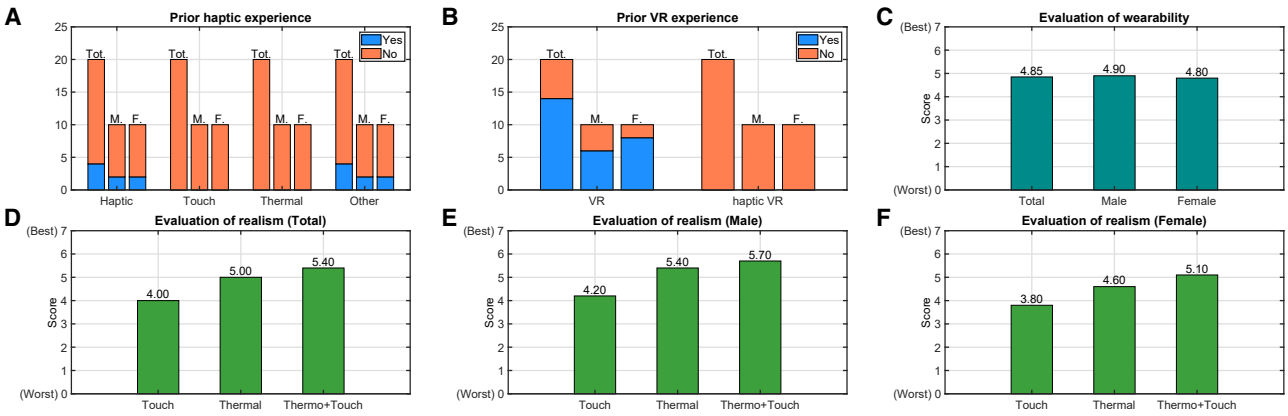

Figure 5. Results of the user test

(A) Prior experiences with haptic feedback devices.

(B) Prior experiences with VR.

(C) User rating for the wearability of the device.

(D–F) User rating for the realism of T^{2}HI by all users, male users, and female users, respectively.

feedback was provided during this stage. In the thermotouch stage, balls of the same color as those in the thermal stage were provided. Touch and thermal feedback were simultaneously provided in four possible combinations: light-warm, light-hot, deep-warm, and deep-hot touches. The effect of contact force on thermal perception was not rigorously considered in the test; the change in thermal resistance between the device and the skin might have influenced the realism of feedback.[47]

Beyond haptic feedback, the maneuverability of the hand is also an important factor for immersion in VR.[48] Therefore, the wearability of the device, that is, the extent to which the hand was unconstrained and comfortable, was assessed (Figure 5C). The grading criteria and results are shown in Table S1. No distinctive difference between the sexes was found, and the wearability of the device was roughly estimated to be unconstrained but still uncomfortable.

Subsequently, the realism of the haptic feedback was assessed (Figures 5D–5F). The efficacy of touch, thermal, and thermotouch feedback was rated from 0 to 7 based on the grading criteria proposed by García-Valle et al. to evaluate the level of realism and artificiality of haptic stimuli in VR.[49] The grading criteria and results are shown in Table S2. The thermotouch haptic feedback received higher scores than the only-touch and only-thermal haptic feedbacks, regardless of gender. Thus, the efficacy of the T^{2}HI in providing a more realistic and immersive haptic VR experience was demonstrated.

DISCUSSION

In this study, we presented a new soft wearable haptic interface, T^{2}HI, to produce both touch and thermal stimuli simultaneously and independently. As base mechanisms for the T^{2}HA, pneumatic actuation (touch feedback) and thermoelectric effect (thermal feedback) were selected owing to their advantages, versatility, and easy implementation on soft wearable haptic feedback devices. A novel design of elastic extension to harmoniously incorporate the different types of components was proposed, and the T^{2}HA successfully performed its task. Additionally, we proposed a wearable pump (YOCP) with a Yoshimura origami pattern. The detailed fabrication process is described in Figure 6. The pump replaced a bulky external pneumatic regulator and compressor without significantly constraining hand motion. A zero-dead-volume pneumatic actuator was also designed to overcome the limited air supply of the YOCP owing to its isolation from the atmosphere. Furthermore, the zero dead volume minimized the thickness of the T^{2}HA, making it more suitable for wearable devices. Finally, T^{2}HI with VR was constructed using the YOCPs and T^{2}HAs. The detailed fabrication of T^{2}HA and the system of T^{2}HI are presented in Figures 7 and 8, respectively. The interface provided six types of haptic feedback for a dynamically interacting virtual object: light, light-warm, light-hot, deep, deep-warm, and deep-hot touches. The efficacy of the T^{2}HI was demonstrated through a user test. Thermotouch haptic feedback was validated to be more realistic and immersive than a single touch or thermal feedback. Furthermore, the device was assessed so as not to heavily constrain hand motion with the equipment, enabling sufficient manual handling of a virtual object in VR. This study demonstrated that integrating diverse types of haptic feedback is crucial for improving the VR experience for humans.

The results of the user test revealed another intriguing implication. Touch feedback was found to be less effective than thermal

Figure 4. Operation of the T^{2}HI

(A–C) Infrared images of thermotouch haptic actuation for no touch, light thermotouch, and deep thermotouch, respectively; see Video S1.

(D) T^{2}HI activity with VR; see Video S2.

(E–G) Interactions with the virtual object. Users can pinch or grab the object in VR.

(H–J) Thermal feedback corresponding to the above hand motion.

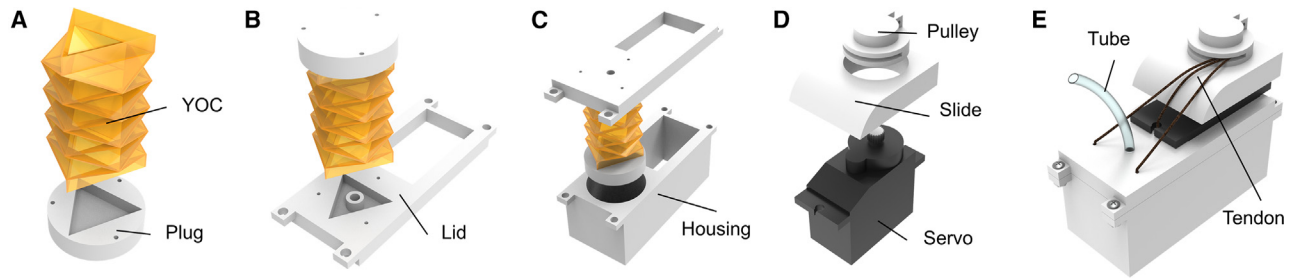

Figure 6. YOCP fabrication

(A) Affixation of a Yoshimura origami cylinder onto a plug.
(B) Affixation of the combined structure onto the lid.
(C) Housing for the YOCP.
(D) Tendon controller with a servo.
(E) The complete assembly of the fabricated YOCP.

feedback in the user test. This can be explained by the different physiological properties of mechanoreceptors and thermoreceptors. Mechanoreceptors receive sensory information from mechanical stimuli induced by physical interactions such as pressure, skin deformation, vibration, etc. Mechanoreceptors are divided into four types according to the type of sensation to be perceived, rate of adaptation, receptive field, and morphology: Merkel discs, Ruffini corpuscles, Meissner corpuscles, and Pacinian corpuscles.[50] In contrast, thermoreceptors are non-specialized neuronal fibers that form ion channels. They have different thresholds and respond to temperature changes rather than to absolute temperatures.[51] Therefore, humans are stricter to touch stimuli than to thermal stimuli. For this reason, users felt that thermal feedback was more effective than touch feedback.

Limitations of the study

The heat accumulation on the opposite surface hampered prolonged cooling feedback, and this is still challenging particularly in wearable haptic devices.[14,33] Due to this limitation, the cool-down could only depend on natural convection. Investigating appropriate heat dissipation methods for soft wearable haptic devices still remains an area for future work.

RESOURCE AVAILABILITY

Lead contact

For additional details and inquiries regarding data sharing, please contact Youngsu Cha (ys02@korea.ac.kr).

Materials availability

This study did not generate new unique reagents.

Data and code availability

- Datasets for this study are available from the corresponding author on reasonable request.
- Codes for this study are available from the corresponding author on reasonable request.
- Other supporting information for this study is available from the corresponding author on reasonable request.

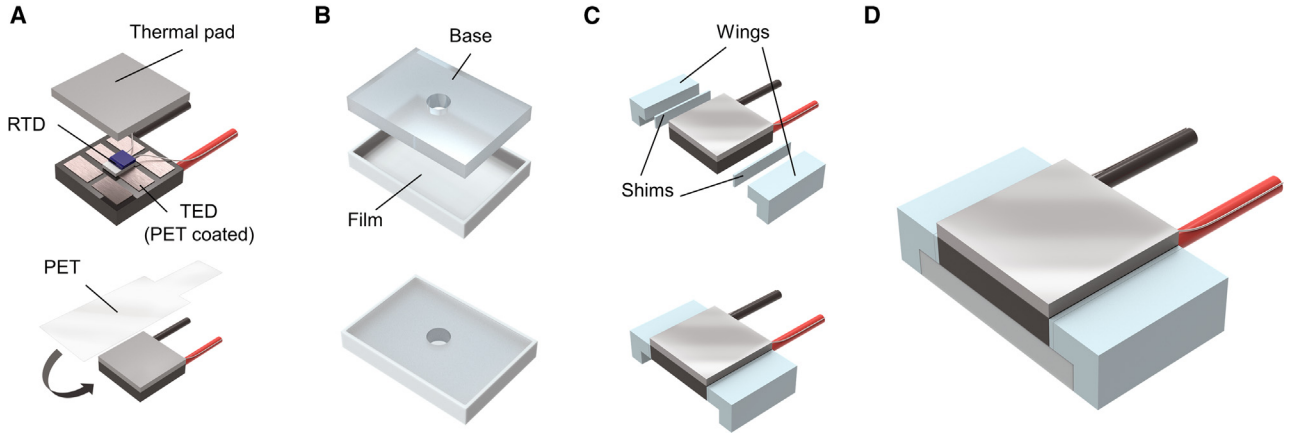

Figure 7. T²HA fabrication

(A) Fabrication of the thermal haptic stimulator.
(B) Fabrication of the touch haptic actuator.
(C) Elastic extension of the thermal haptic stimulator.
(D) The complete assembly of the T²HA fabrication.

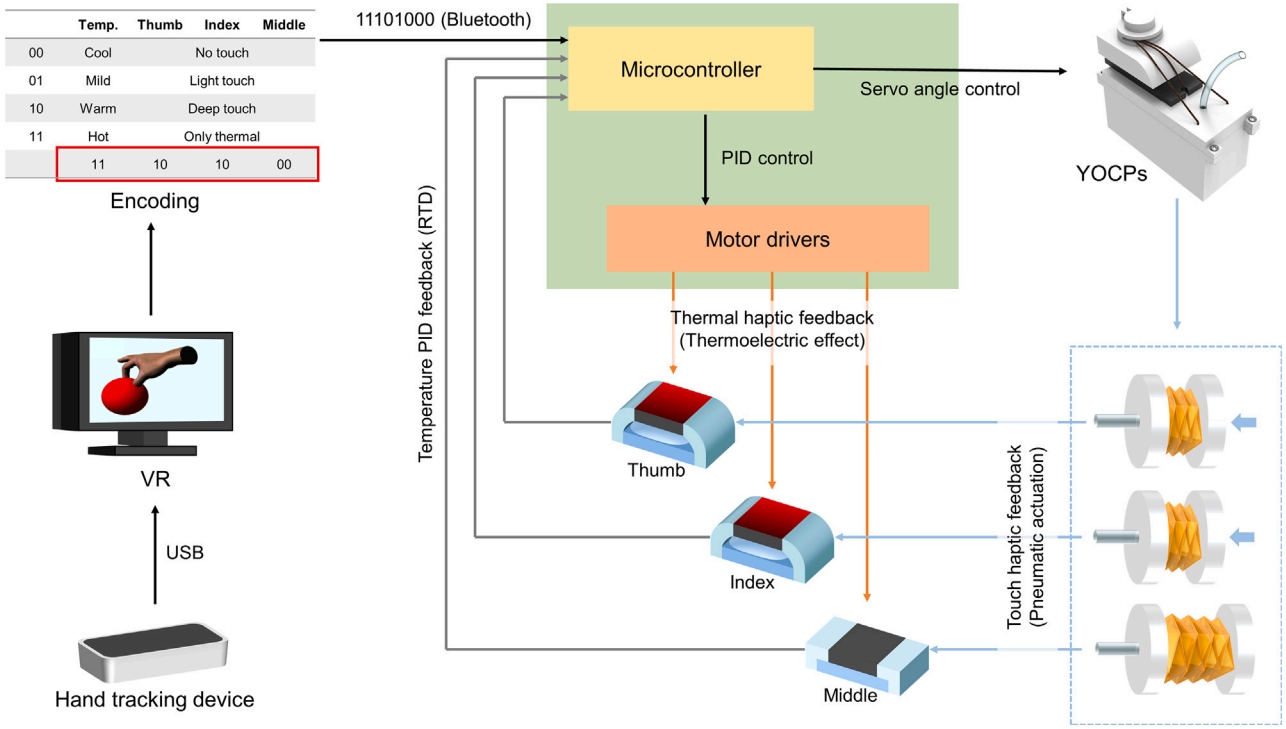

Figure 8. Schematic of the T²HI

This figure shows an example case of the pinch of a hot object with the thumb and index fingers in VR. The state is translated into 1-byte datum 11101000.

ACKNOWLEDGMENTS

This work was supported by the National Research Foundation of Korea through the Ministry of Science and ICT, Korea Government (Grant No. 2022M3C1A3098746). We thank Jiwon Jung for helping draw the illustrations.

AUTHOR CONTRIBUTIONS

S.L. and Y.C. proposed the research subject. S.L. designed the haptic actuators and constructed the total VR interface system. S.L. and S.J. conducted fabrication and experiments. S.L. designed and conducted the user test. S.L. wrote the manuscript, and Y.C. supervised the manuscript writing.

DECLARATION OF INTERESTS

The authors declare no competing interests.

STAR★METHODS

Detailed methods are provided in the online version of this paper and include the following:

- KEY RESOURCES TABLE
- EXPERIMENTAL MODEL AND STUDY PARTICIPANT DETAILS
- METHOD DETAILS
  - YOCP fabrication
  - T²HA fabrication
  - T²HI construction
- QUANTIFICATION AND STATISTICAL ANALYSIS

SUPPLEMENTAL INFORMATION

Supplemental information can be found online at https://doi.org/10.1016/j.isci.2024.111303.

Received: April 30, 2024
Revised: June 18, 2024
Accepted: October 29, 2024
Published: November 1, 2024

REFERENCES

1. Garner, W.R., Hake, H.W., and Eriksen, C.W. (1956). Operationism and the concept of perception. Psychol. Rev. *63*, 149–159. https://doi.org/10.1037/h0042992.
2. Coren, S., Ward, L.M., and Enns, J.T. (2004). Sensation and perception. In Handbook of Psychology, History of Psychology, D.K. Freedheim and I.B. Weiner, eds. (John Wiley & Sons Hoboken), pp. 85–108.
3. Loomis, J.M., and Lederman, S.J. (1986). Tactual perception. In Handbook of Perception and Human Performances, K.R. Boff, L. Kaufman, and J.P. Thomas, eds. (John Wiley & Sons Hoboken).
4. Culbertson, H., Schorr, S.B., and Okamura, A.M. (2018). Haptics: the present and future of artificial touch sensation. Annu. Rev. Control Robot. Auton. Syst. *1*, 385–409. https://doi.org/10.1146/annurev-control-060117-105043.
5. Hayward, V., Astley, O.R., Cruz-Hernandez, M., Grant, D., and Robles-De-La-Torre, G. (2004). Haptic interfaces and devices. Sens. Rev. *24*, 16–29. https://doi.org/10.1108/02602280410515770.
6. Huang, Y., Yao, K., Li, J., Li, D., Jia, H., Liu, Y., Yiu, C.K., Park, W., and Yu, X. (2022). Recent advances in multi-mode haptic feedback technologies

towards wearable interfaces. Mater. Today Phys. *22*, 100602. https://doi.org/10.1016/j.mtphys.2021.100602.

7. Adilkhanov, A., Rubagotti, M., and Kappassov, Z. (2022). Haptic devices: wearability-based taxonomy and literature review. IEEE Access *10*, 91923–91947. https://doi.org/10.1109/ACCESS.2022.3202986.
8. Pacchierotti, C., Sinclair, S., Solazzi, M., Frisoli, A., Hayward, V., and Prattichizzo, D. (2017). Wearable hap tic systems for the fingertip and the hand: taxonomy, review, and perspectives. IEEE Trans. Haptics *10*, 580–600. https://doi.org/10.1109/TOH.2017.2689006.
9. Lederman, S.J., and Klatzky, R.L. (2009). Haptic perception: a tutorial. Atten. Percept. Psychophys. *71*, 1439–1459. https://doi.org/10.3758/APP.71.7.1439.
10. Talhan, A., and Jeon, S. (2018). Pneumatic actuation in haptic-enabled medical simulators: a review. IEEE Access *6*, 3184–3200. https://doi.org/10.1109/ACCESS.2017.2787601.
11. Yin, J., Hinchet, R., Shea, H., and Majidi, C. (2020). Wearable soft technologies for haptic sensing and feedback. Adv. Funct. Mater. *31*, 2007428. https://doi.org/10.1002/adfm.202007428.
12. Ali, H.I., Noor, S., Bashi, S., and Marhaban, M.H. (2009). A review of pneumatic actuators (modeling and control). Aust. J. Basic Appl. Sci. *3*, 440–454.
13. Xavier, M.S., Tawk, C.D., Zolfagharian, A., Pinskier, J., Howard, D., Young, T., Lai, J., Harrison, S.M., Yong, Y.K., Bodaghi, M., and Fleming, A.J. (2022). Soft pneumatic actuators: a review of design, fabrication, modeling, sensing, control and applications. IEEE Access *10*, 59442–59485. https://doi.org/10.1109/ACCESS.2022.3179589.
14. Lee, J., Kim, D., Sul, H., and Ko, S.H. (2021). Thermo-haptic materials and devices for wearable virtual and augmented reality. Adv. Funct. Mater. *31*, 2007376. https://doi.org/10.1002/adfm.202007376.
15. Sonar, H.A., Huang, J.L., and Paik, J. (2021). Soft touch using soft pneumatic actuator-skin as a wearable haptic feedback device. Adv. Intell. Syst. *3*, 2000168. https://doi.org/10.1002/aisy.202000168.
16. Hashem, M.S., Joolee, J.B., Hassan, W., and Jeon, S. (2022). Soft pneumatic fingertip actuator incorporating a dual air chamber to generate multi-mode simultaneous tactile feedback. Appl. Sci. *12*, 175. https://doi.org/10.3390/app12010175.
17. Talhan, A., Kumar, S., Kim, H., Hassan, W., and Jeon, S. (2022). Multimode soft haptic thimble for haptic augmented reality based application of texture overlaying. Displays *74*, 102272. https://doi.org/10.1016/j.displa.2022.102272.
18. Song, K., Kim, S.H., Jin, S., Kim, S., Lee, S., Kim, J.-S., Park, J.-M., and Cha, Y. (2019). Pneumatic actuator and flexible piezoelectric sensor for soft virtual reality glove system. Sci. Rep. *9*, 8988. https://doi.org/10.1038/s41598-019-45422-6.
19. Yu, M., Cheng, X., Peng, S., Cao, Y., Lu, Y., Li, B., Feng, X., Zhang, Y., Wang, H., Jiao, Z., et al. (2022). A self sensing soft pneumatic actuator with closed-Loop control for haptic feedback wearable devices. Mater. Des. *223*, 111149. https://doi.org/10.1016/j.matdes.2022.111149.
20. Sonar, H.A., Gerratt, A.P., Lacour, S.P., and Paik, J. (2020). Closed-loop haptic feedback control using a self-sensing soft pneumatic actuator skin. Soft Robot. *7*, 22–29. https://doi.org/10.1089/soro.2019.0013.
21. Jumet, B., Zook, Z.A., Xu, D., Fino, N., Rajappan, A., Schara, M.W., Berning, J., Escobar, N., Malley, M.K.O., and Preston, D.J. (2022). A textile-based approach to wearable haptic devices. In 2022 IEEE 5th International Conference on Soft Robotics (RoboSoft). https://doi.org/10.1109/RoboSoft54090.2022.9762149.
22. Raitor, M., Walker, J.M., Okamura, A.M., and Culbertson, H. (2017). WRAP: wearable, restricted-aperture pneumatics for haptic guidance. In 2017 IEEE International Conference on Robotics and Automation (ICRA). https://doi.org/10.1109/ICRA.2017.7989055.
23. Kanjanapas, S., Nunez, C.M., Williams, S.R., Okamura, A.M., and Luo, M. (2019). Design and analysis of pneumatic 2-doF soft haptic devices for shear display. IEEE Rob. Autom. Lett. *4*, 1365–1371. https://doi.org/10.1109/LRA.2019.2895890.
24. Kim, S.-W., Kim, S.H., Kim, C.S., Yi, K., Kim, J.-S., Cho, B.J., and Cha, Y. (2020). Thermal display glove for interacting with virtual reality. Sci. Rep. *10*, 11403. https://doi.org/10.1038/s41598-020-68362-y.
25. Maeda, T., and Kurahashi, T. (2019). TherModule: wearable and modular thermal feedback system based on a wireless platform. In Proceedings of the 10th Augmented Human International Conference 2019. https://doi.org/10.1145/3311823.3311826.
26. Lee, Y., Lim, H., Kim, Y., and Cha, Y. (2021). Thermal feedback system from robot hand for telepresence. IEEE Access *9*, 827–835. https://doi.org/10.1109/ACCESS.2020.3047036.
27. Tewell, J., Bird, J., and Buchanan, G.R. (2017). The heat is on: a temperature display for conveying affective feedback. In Proceedings of the 2017 CHI Conference on Human Factors in Computing Systems (Association for Computing Machinery). https://doi.org/10.1145/3025453.3025844.
28. Lee, J., Sul, H., Lee, W., Pyun, K.R., Ha, I., Kim, D., Park, H., Eom, H., Yoon, Y., Jung, J., et al. (2020). Stretchable skin-like cooling/heating device for reconstruction of artificial thermal sensation in virtual reality. Adv. Funct. Mater. *30*, 1909171. https://doi.org/10.1002/adfm.201909171.
29. Wettach, R., Behrens, C., Danielsson, A., and Ness, T. (2007). A thermal information display for mobile applications. In Proceedings of the 9th International Conference on Human Computer Interaction with Mobile Devices and Services (Association for Computing Machinery). https://doi.org/10.1145/1377999.1378004.
30. Parida, K., Bark, H., and Lee, P.S. (2021). Emerging thermal technology enabled augmented reality. Adv. Funct. Mater. *31*, 2007952. https://doi.org/10.1002/adfm.202007952.
31. Jung, Y.H., Kim, J.-H., and Rogers, J.A. (2021). Skin-integrated vibrohaptic interfaces for virtual and augmented reality. Adv. Funct. Mater. *31*, 2008805. https://doi.org/10.1002/adfm.202008805.
32. Oh, J., Kim, S., Lee, S., Jeong, S., Ko, S.H., and Bae, J. (2021). A liquid metal based multimodal sensor and haptic feedback device for thermal and tactile sensation generation in virtual reality. Adv. Funct. Mater. *31*, 2007772. https://doi.org/10.1002/adfm.202007772.
33. Pyun, K.R., Rogers, J.A., and Ko, S.H. (2022). Materials and devices for immersive virtual reality. Nat. Rev. Mater. *7*, 841–843. https://doi.org/10.1038/s41578-022-00501-5.
34. Yu, X., Xie, Z., Yu, Y., Lee, J., Vazquez-Guardado, A., Luan, H., Ruban, J., Ning, X., Akhtar, A., Li, D., et al. (2019). Skin-integrated wireless haptic interfaces for virtual and augmented reality. Nature *575*, 473–479. https://doi.org/10.1038/s41586-019-1687-0.
35. Cai, S., Ke, P., Narumi, T., and Zhu, K. (2020). ThermAirGlove: a pneumatic glove for thermal perception and material identification in virtual reality. In 2020 IEEE Conference on Virtual Reality and 3D User Interfaces (VR) (IEEE). https://doi.org/10.1109/VR46266.2020.00044.
36. Lee, E.-H., Kim, S.-H., and Yun, K.-S. (2021). Three-axis pneumatic haptic display for the mechanical and thermal stimulation of a human finger pad. Actuators *10*, 60. https://doi.org/10.3390/act10030060.
37. Wang, D., Guo, Y., Liu, S., Zhang, Y., Xu, W., and Xiao, J. (2019). Haptic display for virtual reality: progress and challenges. Virtual Real. Intell. Hardw. *1*, 136–162. https://doi.org/10.3724/SP.J.2096-5796.2019.0008.
38. Giri, G.S., Maddahi, Y., and Zareinia, K. (2021). An application-based review of haptics technology. Robotics *10*, 29. https://doi.org/10.3390/robotics10010029.
39. Sun, Z., Zhu, M., Shan, X., and Lee, C. (2022). Augmented tactile-perception and haptic-feedback rings as human-machine interfaces aiming for immersive interactions. Nat. Commun. *13*, 5224. https://doi.org/10.1038/s41467-022-32745-8.

40. Kim, Y., and Cha, Y. (2020). Soft pneumatic gripper with a tendon-driven soft origami pump. Front. Bioeng. Biotechnol. *8*, 461. https://doi.org/10.3389/fbioe.2020.00461.

41. Yoshimura, Y. (1955). On the Mechanism of Buckling of a Circular Cylindrical Shell under Axial Compression (National Advisory Committee for Aeronautics).

42. Zhang, Q., Fang, H., and Xu, J. (2021). Yoshimura-origami based earthworm-like robot with 3-dimensional locomotion capability. Front. Robot. AI *8*, 738214. https://doi.org/10.3389/frobt.2021.738214.

43. Zhou, Y., Yu, H., Xu, S., Luo, M., and Zhou, X. (2022). High-density thermal sensitivity of the hand under different thermal states and stimulus intensities. Indoor Air *32*, e13089. https://doi.org/10.1111/ina.13089.

44. Guergova, S., and Dufour, A. (2011). Thermal sensitivity in the elderly: a review. Ageing Res. Rev. *10*, 80–92. https://doi.org/10.1016/j.arr.2010.04.009.

45. Abdouni, A., Vargiolu, R., and Zahouani, H. (2018). Impact of finger biophysical properties on touch gestures and tactile perception: aging and gender effects. Sci. Rep. *8*, 12605. https://doi.org/10.1038/s41598-018-30677-2.

46. Gerrett, N., Ouzzahra, Y., Coleby, S., Hobbs, S., Redortier, B., Voelcker, T., and Havenith, G. (2014). Thermal sensitivity to warmth during rest and exercise: a sex comparison. Eur. J. Appl. Physiol. *114*, 1451–1462. https://doi.org/10.1007/s00421-014-2875-0.

47. Galie, J., Ho, H.N., and Jones, L.A. (2009). Influence of contact conditions on thermal responses of the hand. In World Haptics 2009- Third Joint EuroHaptics Conference and Symposium on Haptic Interfaces for Virtual Environment and Teleoperator Systems. https://doi.org/10.1109/WHC.2009.4810902.

48. Monteiro, P., Gonçalves, G., Coelho, H., Melo, M., and Bessa, M. (2021). Hands-free interaction in immersive virtual reality: asystematic review. IEEE Trans. Vis. Comput. Graph. *27*, 2702–2713. https://doi.org/10.1109/TVCG.2021.3067687.

49. García-Valle, G., Ferre, M., Breñosa, J., and Vargas, D. (2017). Evaluation of presence in virtual environments: haptic vest and user's haptic skills. IEEE Access *6*, 7224–7233. https://doi.org/10.1109/ACCESS.2017.2782254.

50. Johnson, K.O. (2001). The roles and functions of cutaneous mechanoreceptors. Curr. Opin. Neurobiol. *11*, 455–461. https://doi.org/10.1016/S0959-4388(00)00234-8.

51. Zhang, X. (2015). Molecular sensors and modulators of thermoreception. Channels *9*, 73–81. https://doi.org/10.1080/19336950.2015.1025186.

STAR★METHODS

KEY RESOURCES TABLE

REAGENT or RESOURCE	SOURCE	IDENTIFIER
Software and algorithms		
MATLAB (MATLAB R2023b)	MathWorks Inc., USA	N/A
3D CAD (Fusion 360)	Autodesk Inc., USA	N/A
Openframeworks	https://openframeworks.cc/	N/A
Other		
Laser sensor (IL-100 CMOS multifunction analog laser sensor)	Keyence Co., Japan	N/A
Pressure sensor (33A-015D-2210)	Shiba Korea Co., Ltd., Korea	N/A
Data acquisition board (DAQ NI-9229)	National Instrument Co., USA	N/A
Tensile compression testing machine (MCT-2150)	A&D Co., Ltd., Japan	N/A
DC power supply (MK3003P)	MKPOWER Co. Ltd., Korea	N/A
Infrared camera (FLIR A-700)	FLIR Systems Inc., USA	N/A
Hand tracking device (Leap Motion Controller)	Leap Motion, Inc., USA	N/A
Overhead projector film	Copier Land Co., Ltd., Korea	N/A
Laser cutter (Epilog Fusion Edge - RF30w)	Epilog Laser Co., USA	N/A
Kapton tape (3M™ Polyimide Tape 8997)	3M Co., USA	N/A
Epoxy glue (3M™Scotch-Weld™ Epoxy Adhesive DP460)	3M Co., USA	N/A
Servo motor (MG90D)	Tower Pro Pte. Ltd.	N/A
Silpoxy (Sil-Poxy™)	Smooth-On Inc., USA	N/A
Thermoelectric device (Flexible Thermoelectric Device)	Tegway Co., Ltd., Korea	N/A
Resistance temperature detector (PT1000B00-FC1-N00)	Sentrion Co., Korea	N/A
Polydimethylsiloxane (SYLGARD™ 184 Silicone Elastomer)	Dow Inc., USA	N/A
Ecoflex (Ecoflex 0030)	Smooth-On Inc., USA	N/A
Cyanoacrylate adhesive (AXIA-2700)	Alteco Korea Inc., Korea	N/A

EXPERIMENTAL MODEL AND STUDY PARTICIPANT DETAILS

The user test for this study was approved by the Korea University Institutional Review Board (Approval Number: KUIRB-2023-0387-01). Twenty Korean participants in their 20s (10 male and 10 female) participated voluntarily in the test with informed consent. No significant difference between genders was found.

METHOD DETAILS

YOCP fabrication

The YOCP was designed using Fusion 360 software (Autodesk Inc., USA). The Yoshimura origami cylinder was initially fabricated through the process described in Figure S2. First, the Yoshimura pattern was carved on a 100 μm overhead projector (OHP) film (Copier Land Co., Ltd., Korea) using a laser cutter (Epilog Fusion Edge- RF30w, Epilog Laser Co., USA), with the specific parameters for full flat transformation[42]; the pattern is shown in Figure S2A with the parameters of $L = 10$ mm, $h = 3$ mm, and $\alpha = 30°$. Second, the carved OHP film was rolled into a cylindrical shell such that the carved side was on the inside, and wrapped by Kapton tapes (3M Polyimide Tape 8997, 3M Co., USA) three times, considering the axis symmetry of the cylinder (Figure S2B). Multi-overlaid tapping

was performed to ensure a secure pump sealing. Finally, the tapped cylinder was folded along the carved lines to form a Yoshimura origami cylinder.

The YOCP was fabricated through the process shown in Figure 6. In the fabrication, all affixations are done using epoxy glue (3MScotch-Weld Epoxy Adhesive DP460, 3M Co., USA), and the material used for all the components was acrylonitrile butadiene styrene (ABS) plastic. First, one side of the Yoshimura origami cylinder was affixed to a 3-mm-deep triangular blind hole with a 14 mm diameter × 4 mm height plug (Figure 6A). Second, the other side of the cylinder was affixed to a 3-mm-deep triangular blind hole with a 17 mm width × 42 mm length × 4 mm height lid (Figure 6B). Third, the affixed (both top and bottom) cylinders were inserted into a 15 mm diameter × 16 mm depth circular blind hole with a 17 mm width × 42 mm length × 17 mm height housing (Figure 6C). Fourth, a tendon controller with a servo (MG90D, Tower Pro Pte. Ltd.) was made (Figure 6D). A 17 mm width × 24 mm length × 6.5 mm height block with a smooth slide was affixed to the servo. Then, a 4-mm-groove-diameter pulley was affixed to the gear of the servo. Finally, all the parts were assembled (Figure 6E). A tendon was anchored to the pulley and looped through three 1-mm-diameter holes of the plug and lid to encircle the cylinder. The tendon controller was inserted into a 12.2 mm width × 23 mm length × 14 mm depth rectangular blind hole of the housing through a 4-mm-depth rectangular hole in the lid. The lid and housing were fastened to M2-size bolts and nuts. A 2 mm diameter × 25 cm length silicone tube was affixed into a 2-mm-diameter hole on the lid using silpoxy (Sil-Poxy, Smooth-On Inc., USA).

T^2HA fabrication

The T^2HA and molds for silicone casting were designed using Fusion 360 software. T^2HA was fabricated through the process described in Figure 7. First, a thermal haptic stimulator was fabricated (Figure 7A). The TED (Flexible Thermoelectric Device, Tegway Co., Ltd., Korea) was presented by Kim et al., and they confirmed the cooling capacity reaches a maximum $-10^{\circ}C$[24]. A 10 mm width × 10 mm length × 2.3 mm thickness TED was coated by a 10 mm width × 10 mm length × 20 μm thickness polyethylene terephthalate (PET) tape for electric insulation. A 2.0 mm width × 2.3 mm length × 1.1 mm thickness RTD (PT1000B00-FC1-N00, Sentrion Co., Korea) was mounted on the PET-coated TED. A thermal pad was used to cover the TED and RTD for even heat diffusion on the surface. PET tape was used to wrap the sandwiched components to fix them firmly. Next, a touch haptic actuator was fabricated (Figure 7B). A 14 mm width × 9 mm length × 2 mm thickness inelastic base of the pneumatic actuator was made from polydimethylsiloxane (PDMS) (SYLGARD 184 Silicone Elastomer, Dow Inc., USA). An elastic film was obtained from Ecoflex (Ecoflex 0030, Smooth-On Inc., USA). The film was shaped into a cuboid cap with a uniform 0.5 mm thickness across all surfaces, which fully covered the base without any gaps. The base and film were glued together by applying silpoxy to the four facets of the base. The opposite end of the silicone tube of the YOCP was connected to the 2-mm-diameter hole in the base using silpoxy. Third, the thermal haptic stimulator was extended elastically (Figure 7C). Two 0.5-mm-thickness shims made from Ecoflex were attached to both sides of the TED of the thermal haptic stimulator using cyanoacrylate adhesive with primer (AXIA-2700, Alteco Korea Inc., Korea). Two elastic wings made from Ecoflex were affixed to the shims using silpoxy. The shims provide new surfaces on which the silploxy can be applied, which has a longer working time than the cyanoacrylate adhesive; the instant working time of the cyanoacrylate adhesive makes it difficult to successfully attach the highly flexible wings onto the narrow facets of the TED at once. Finally, the elastically extended thermal haptic stimulator and the touch haptic actuator were combined into the T^2HA (Figure 7). They were affixed by applying silpoxy to the sides of the touch haptic actuator. The weight of a single T^2HA unit with the YOCP was 35 g.

T^2HI construction

The T^2HI was constructed using YOCPs and T^2HAs. The VR environment for the T^2HI was created based on the openFrameworks, a C++ open-source software development toolkit. A Schematic of the T^2HI is shown in Figure 8. A hand tracking device (Leap Motion Controller, Leap Motion Inc., USA) was used to measure the position and orientation of the bones of the real hand, and the data were transmitted via universal serial bus (USB) communication to the VR. The data were manipulated to update the real-time skeleton animation of the virtual hand. Along with the skeletons of the virtual hand, physical bodies were created and updated. The physical bodies of the virtual hand tangibly interacted with a virtual object. Because T^2HAs were worn on the fingertips of the thumb, index, and middle fingers, only the collision data on these parts were considered. In turn, the collisions between each physical body and the object were encoded into 1-byte data with four 2-bit segments. The first 2-bit segment represented the temperature level of the object. The cool, mild, warm, and hot temperature levels were assigned values of 00, 01, 10, and 11, respectively. The other three segments were related to the intensity of touch, which was determined by the collision depth between the physical skeleton of the virtual hand and object. The no touch, light touch, deep touch, and only-thermal stimulation states were assigned as 00, 01, 10, and 11, respectively. The 1-byte contact data were transmitted to the microcontroller via the Bluetooth communication. The microcontroller decoded the data, which were then translated into the manipulation states of the YOCPs and motor drivers. The no touch and only thermal states were translated into no servo rotation, the light touch state was translated into a 60° servo rotation, and the deep touch state was translated into a 120° servo rotation. Target temperatures corresponding to the temperature levels were set in the microcontroller; for example, warm and hot temperature levels were set to $37^{\circ}C$ and $40^{\circ}C$ in the user test. According to the target temperature, the duty of the motor driver was continuously calculated based on the current temperature measured by the RTD of the T^2HA. The mild temperature level was translated into zero duty such that no thermal feedback was provided.

QUANTIFICATION AND STATISTICAL ANALYSIS

The MATLAB software was used for the statistical analysis of this study. The averages and standard deviations for male (n = 10), female (n = 10), and the total (n = 20) were calculated. The results were shown in Figure 5, Tables S1 and S2.